ScienceAdvances

www.advances.sciencemag.org/cgi/content/full/1/2/e1400083/DC1

Supplementary Materials for

The mobility of single-file water molecules is governed by the number of H-bonds they may form with channel-lining residues

Andreas Horner, Florian Zocher, Johannes Preiner, Nicole Ollinger, Christine Siligan, Sergey A. Akimov, Peter Pohl*

Published 20 March 2015, *Sci. Adv.* **1**, e1400083 (2015)
DOI: 10.1126/sciadv.1400083

This PDF file includes:

Supplemental material:

The mobility of single-file water molecules is governed by the number of H-bonds they may form with channel-lining residues

Andreas Horner, Florian Zocher, Johannes Preiner, Nicole Ollinger, Christine Siligan, Sergey A. Akimov, Peter Pohl

Dependence of vesicle volume on P_f

In order to determine water mobility within the channels, we subjected the reconstituted vesicles to osmotic stress. The rate of vesicle shrinkage depends on the permeability of the vesicular membrane P_f:

$$\frac{dV(t)}{dt} = AP_f V_w \left(\frac{V_0}{V(t)} c_0^i - \left(c_0^i + c_S \right) \right) \tag{S1}$$

where V_w, V_0, A, c_0[1] and c_s are the molar volume of water, vesicle volume at time zero, surface area of the vesicle, the initial osmolyte concentration inside the vesicles, and the incremental osmolyte concentration in the external solution due to sucrose addition, respectively. The analytical solution of Eq. (S1) is given in the main text as Eq. 2.

Dependency of scattered light intensity on vesicle volume

V(t) is experimentally accessible by measuring I(t). To derive the corresponding expression, we exploited the Rayleigh-Gans-Debye relation (*1*):

$$I \sim \left(\frac{\lambda^2}{4\pi^2} \right) \left(\frac{m^2 - 1}{m^2 + 2} \right)^2 \delta^6 \left(\frac{1 + \cos^2 \theta}{2} \right) P(\theta) \tag{S2}$$

where λ, θ, m, δ, $P(\theta)$ are the effective wavelength (i.e. the ratio of λ_0 (=546 nm in our experiments) and the refractive index n_S of the aqueous solution (with sucrose), the angle (here 90°) at which the intensity I of scattered light was measured, the relative refractive index ($m = n_p/n_s$, where n_p is the average refractive index of the particle), the size parameter, and the form-factor, respectively. δ is defined as $\delta = 2\pi R / \lambda$, where R is the vesicle radius. The optically homogeneous vesicles $P(\theta)$ may be expressed via $P(\theta) = (3(\sin u - u \cos u)/u^3)^2$ where u = 2δsin(θ/2).

In order to get an explicit expression for I in Eq. (S2), we first obtained an average refractive index n_p of the particles from the equation:

$$\frac{n_p^2 - 1}{n_p^2 + 2} = f \frac{n_L^2 - 1}{n_L^2 + 2} + (1 - f) \frac{n_e^2 - 1}{n_e^2 + 2} \tag{S3}$$

where n_L=1.497 (*1*), n_e, and f are the refractive indices of the lipid, the intravesicular solution, and the volume fraction of the lipids per vesicle, respectively. Expressing f as a function of R_0, R, and h, i.e. the initial vesicle radius, the effective radius of the osmotically-squeezed vesicles, and the membrane thickness ≈ 4 nm, respectively:

$$f = \frac{4\pi R_0^2 h}{\frac{4}{3}\pi R^3} = \frac{3R_0^2 h}{R^3} \tag{S4}$$

results in an expression for n_p:

$$n_p = \sqrt{\frac{R^3\left(2+n_L^2\right)n_e^2 + 6R_0^2 h\left(n_L^2 - n_e^2\right)}{R^3\left(2+n_L^2\right) - 3R_0^2 h\left(n_L^2 - n_e^2\right)}} \tag{S5}$$

Vesicle shrinkage increases the internal electrolyte concentration. Thus, n_e also increases:

$$n_e = n_e^0 + \left(\frac{\partial n_e}{\partial c}\right)\Delta c = n_e^0 + \mu_c c_0\left(\frac{R_0^3}{R^3} - 1\right) \tag{S6}$$

where n_e^0, c_0 = 0.6 wt % (100 mM NaCl, 20 mM MOPS), and $\mu_c \approx 1.7 \cdot 10^{-3}$ are the initial refractive index, the initial solute concentration, and the concentration coefficient for the refractive index.
The refractive indices n_S of the external solution amount to 1.3354, 1.3380, 1.3403, 1.3433, and 1.3479 for increasing sucrose concentrations of 50, 100, 150, 200, and 300 mM, respectively. To account for the temperature dependence of n_e and n_s we used:

$$n_T = n_{20} + \left(\frac{\partial n}{\partial T}\right)\Delta T = n_{20} + \mu_T \Delta T \tag{S7}$$

where n_{20}, n_T, and $\mu_T = -1.2 \cdot 10^{-4}$ K^{-1} (*2*) are the refractive index at 20 °C, the refractive index at a given temperature T, and the temperature coefficient for the refractive indices, respectively.

By using Eqs. S2-S7 and assuming a proportionality coefficient of unity, we have plotted the functions $I(R)$ and $I(V)$, for $\theta = \pi/2$ (Fig. S1).

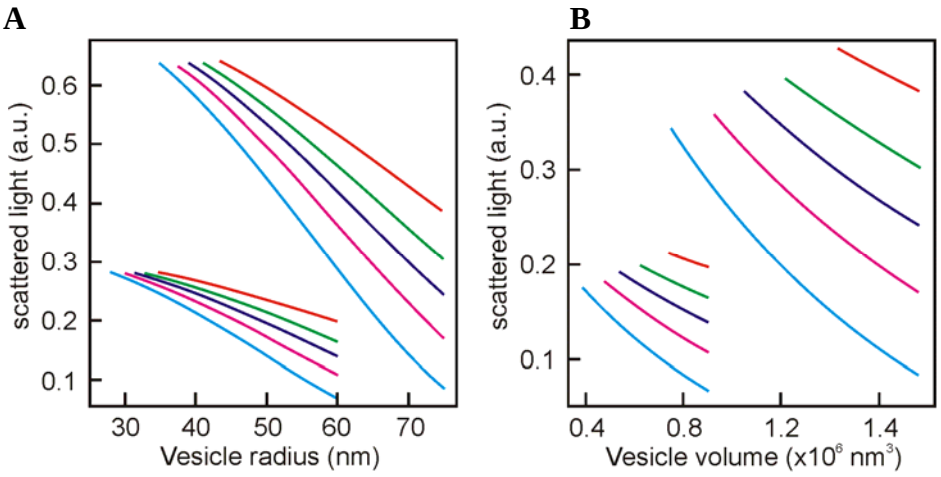

Fig. S1. The intensity I of scattered light for osmotically-challenged vesicles as a function of vesicle radius R **(A)** and vesicle volume V **(B)**. Each panel shows two different populations of vesicles: with initial radii R_0 of 60 and 75 nm. Vesicles of these radii result from extrusion through pores with a diameter of 100 nm and 200 nm, respectively (*3*). The osmotic pressure was generated by external sucrose concentrations of 50 (red), 100 (green), 150 (blue), 200 (magenta), 300 (cyan) mM.

The dependency of scattered light intensity I on R but not on V exhibits inflection points (Fig. S1). As a consequence, substitution of Eq. (S2) for its Taylor series should be more accurate for $I(V)$. SFig. 2 confirms this prediction. To maintain the desired level of accuracy, we thus used the Taylor expansion for *I(V)* (Fig. S2):

$$I(t) = a + bV(t) + dV^2(t) \tag{S8}$$

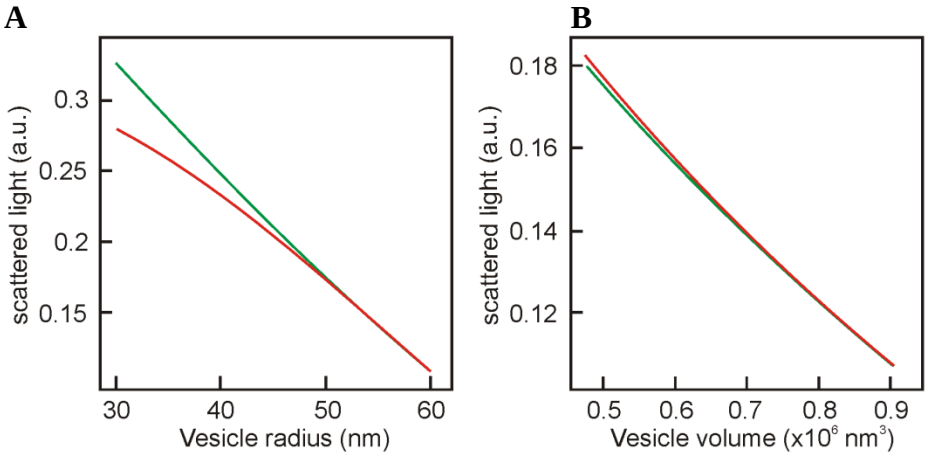

Fig. S2. Comparison of the exact dependencies for I (red) with the approximate representations by their Taylor series (green) for R: $I(t) = a + bR(t) + dR^2(t)$ ***(A)*** or for V: $I(t) = a + bV(t) + dV^2(t)$ ***(B)***. The calculations were done for vesicles that were extruded through 100-nm filters and a sucrose concentration of 200 mM.

Osmotically-induced vesicle shrinkage resulted in an increase of I. The time course depended on the size of the vesicles, i.e. it was different for extrusion filters with diameters of 100 and 200 nm. We inserted Eq. 2 into Eq S8 and fitted the resulting expression to the data points (Fig. S3).

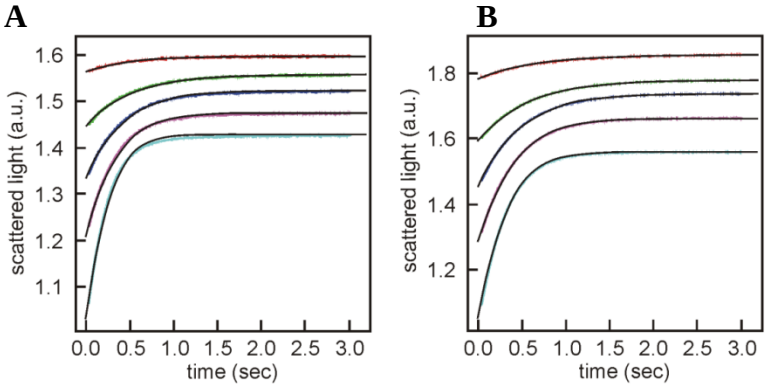

Fig. S3. Osmotically-induced vesicle shrinkage was accompanied by an increase in I. The vesicles were prepared by extrusion through 100 ***(A)*** or 200 nm ***(B)*** wide pores. The color code for the external sucrose concentrations is as in SFig. 1. A global fit of Eq. (S8) to all data in **(A)** and to all data in **(B)** resulted in P_f values of 4.3 µm/s and 4.6 µm/s, respectively.

We then measured the osmotically-induced shrinkage of proteoliposomes using a stopped-flow apparatus with a dead time of 2.6 ms under the particular experimental conditions. In order to increase the accuracy of $P_{f,c}$ determination, we performed the stopped-flow experiments for different numbers n of functional AQP units per vesicle. Fig. S4 shows the dependence of normalized scattered light intensity on time.

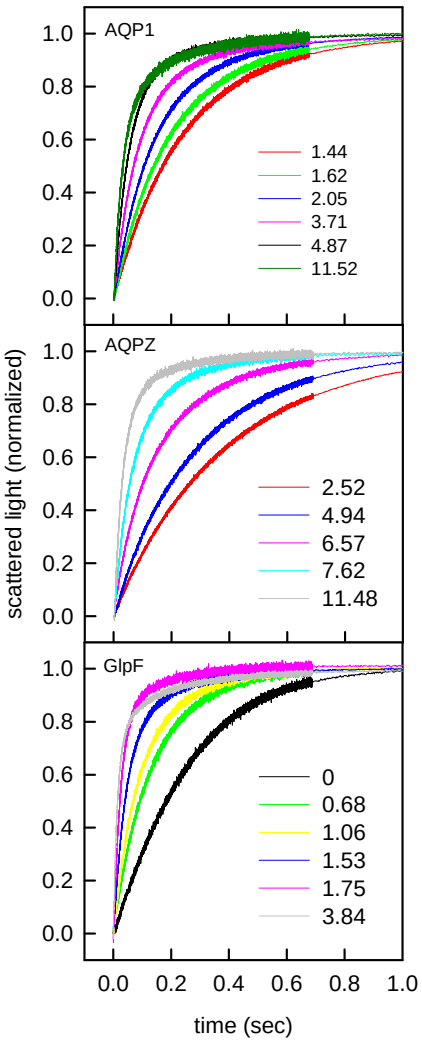

Fig. S4 Osmotic shrinkage of proteoliposomes. Normalized stopped flow data for all three aquaporins. Equal volumes of vesicle suspension and hyperosmotic solution (c_{osm} = 150mM sucrose) were mixed. Both syringes contained 100mM NaCl, 20mM MOPS (pH 7.4, at 5°C). The number of reconstituted AQP monomers per proteoliposome is indicated.

Comparison of AFM and FCS-based protein detection

As AqpZ was exclusively detected as tetramers in FCS measurements, the numbers detected via FCS and AFM can be directly compared. In the case of AQP1 and GlpF, smaller oligomers (dimers or trimers) have been detected via FCS. Since the AFM resolution on this scale (400x400 nm^2) is too low to discriminate tetramers from trimers, dimers, and monomers, only the number of oligomers per liposome can be detected. However, we can still compare the FCS values (=mean number of monomers per liposome, $N_{M,FCS}$) to the AFM values (mean number of oligomers per liposome, $N_{O,AFM}$) by assuming that the number of monomers k=0,1,2,3,… per liposome is described by a Poisson distribution with mean $N_{M,FCS}$:

$$P^{N_{M,FCS}}(k) = \frac{N_{M,FCS}^{k}}{k!} e^{-N_{M,FCS}} \qquad \text{(S9)}$$

and by assuming that the affinity of a monomer for another monomer is high enough so that all monomers per liposome arrange themselves into the smallest possible number of oligomers $n(k)$= 0,1,1,1,1,2,2,2,2,3,3,…. In this way we can calculate the number of particles (oligomers) per liposome that would be detected by AFM for a given number of monomers detected via FCS by:

$$N_{O,FCS} = \sum_{k} P^{N_{M,FCS}}(k) \cdot n(k) \qquad \text{(S10)}$$

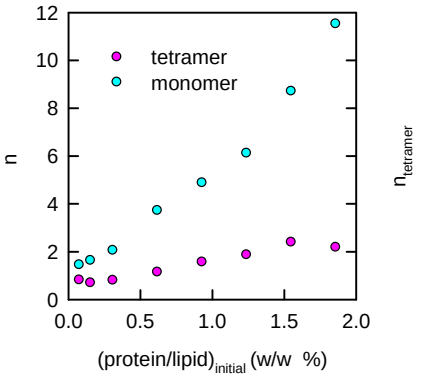

Fig. S5. A typical FCS counting experiment of an AQP1-YFP reconstitution series. The number *n* of reconstituted AQP1 monomers and the number of reconstituted AQP1 tetramers $n_{tetramer}$ increases with the protein/lipid ratio that was used for reconstitution. The number of tetramers per proteoliposome (pink dots) is deduced from the ratio of fluorescent particles before and after the addition of octyl glucoside to the liposome suspension. In contrary, vesicles dissolved in octyl glucoside and sodium dodecyl sulfate resulted in AQP1-YFP monomers (cyan dots).

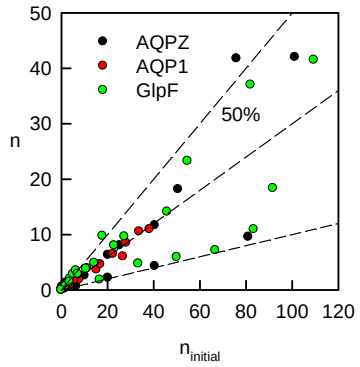

Fig. S6. Reconstitution efficiency varied between 10% and 50%. The initial number $n_{initial}$ of AQP monomers per vesicle was calculated from FCS experiments of purified AQPs in solution and the amount of lipid used for the reconstitution. We presumed a vesicle diameter of 120 nm after extrusion through a 100 nm polycarbonate filter. The dashed black lines should help to guide the eye.

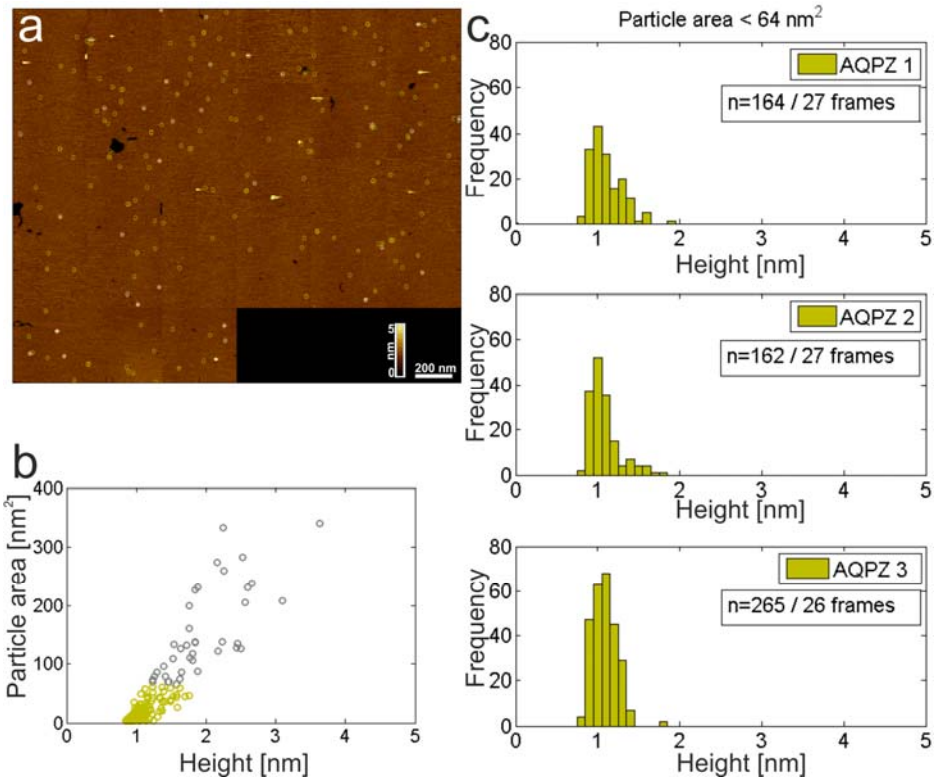

Fig. S7. Membrane protein detection by AFM. (a) Proteoliposomes (in this case containing AQPZ) were spread on freshly cleaved mica. 25-30 images (400x400 nm^2) at different positions on the sample were recorded. A height threshold of 3 times the standard deviation of the supported lipid bilayer (0.7 nm) was used to automatically detect particles embedded in the bilayer. (b) Area vs. mean height of detected particles. A cluster of uniform particles with areas below ~64 nm^2 can be observed. This cluster is interpreted as a cluster of AQPZ tetramers broadened by the finite radius of the AFM tip. (c) Histograms of average height values from particles (area < 64 nm^2) that were obtained in three different reconstitutions.

Table S1. Overview of published *in vitro* and *in silico* single-channel permeability values p_f for AQP1, GlpF and AqpZ as discussed in the main text.

Reference	T [K]	$p_{f,AQP1}$ [10^{-14} cm^3/s]	$k_{0,AQP1}$ [10^9 s^{-1}]	$p_{f,GlpF}$ [10^{-14} cm^3/s]	$k_{0,GlpF}$ [10^9 s^{-1}]	$p_{f,AqpZ}$ [10^{-14} cm^3/s]	$k_{0,AqpZ}$ [10^9 s^{-1}]
(*4*)	310			14±1	*4.7±0.3*		
(*5*)	310	7.1±0.9	*2.4±0.3*				
(*6*)	300	10±4	*3.4±1.3*	16±3	*5.4±1*	16±5	*5.4±1.7*
	310			8.6±1.1–13.1±3.4	*2.9±0.4 – 4.4±1.1*	3.2±0.7–4.4±0.7	*1.1±0.2 – 1.5±0.2*
(*7*)	300	*9*	3	*3*	1		
(*8*)	310			*3.3*	1.1		
(*9*)	295	5.43	*1.82*				
(*10*)	295	1.4	*0.47*				
This paper	298	52.8±4.7	*17.7±1.6*	190±27.8	*63.5±9.3*	28.8±2	*9.6±0.6*

A note on unstirred layer effects in previously reported experiments

Giant vesicles containing AQP1 have been measured for only a single protein concentration. p_f amounted to only ~1/5 of our value at 5 °C due to the unaccounted presence of unstirred layers. That is, the osmotic flow through both the unavoidably present internal and external stagnant near-membrane layers resulted in osmolyte dilution (*11*) adjacent to the outer leaflet and a non-uniform distribution of the self-quenching dye (whose fluorescence was used as the read-out for the volume change) within the shrinking vesicle. We may estimate the time required for equilibrating the intravesicular dye concentration by calculating the time τ_s that a dye with a diffusion constant of D_{dye}=4.36x10^{-6}cm^{2}s^{-1} (*12*) requires to cross r_{sv}~1.2 µm (= the radius of the shrunken vesicle) by diffusion: $\tau_s = r_{sv}^2/6D_{dye}$ = 0.5 ms. Assuming (i) the sizes of the outer and the inner unstirred layers are equal and (ii) that sucrose and carboxyfluorescein have the same mobility in water, we find that it takes sucrose about 0.5 ms to reach the vesicular membrane. Sucrose diffusion and subsequent dye equilibration started only after the proteoliposomes had been mixed with the hypertonic solution. Assuming that this takes one more millisecond, we arrive at a time interval of 2 ms, during which the fluorescence is governed by processes different from membrane water permeation. Since it took the giant vesicles only 3.7 ms to shrink (*9*), the limiting effect of the mixing and diffusion processes during the first 2 ms cannot be ignored. Most likely, they account for the underestimation of p_f in (*9*).

In the other experiment, electron microscopy was exploited to count water channels that were located in the membrane of AQP1 overexpressing oocytes (*10*). Due to the large cell size, unstirred layers were also likely to have hampered these measurements. The assumption of an invariant internal unstirred layer of 100 µm thickness and a cytoplasmic water diffusion coefficient of 10^{-5} cm^{2}s^{-1} returns an unstirred layer water permeability of P_{UL}=10^{-5} cm^{2}s^{-1}/10^{-2} cm=10^{-3} cm/s, which roughly coincides with the apparent water permeability P_a that was measured. Since

$$1/P_a=1/P_f+1/P_{UL}, \qquad \text{(S11)}$$

P_a was determined by P_{UL} and did not reflect P_f>P_{UL}. Thus, the p_f=1.4 x 10^{-14}cm^{3}s^{-1} which was derived from P_a (*10*) was, in all likelihood, also an underestimation.

This has not been recognized previously, because P_a linearly increased with n instead of asymptotically approaching P_{UL} (*10, 13*). The apparent contradiction to Eq. S11 vanishes if the dependence of P_{UL} on vesicle volume is taken into account: Osmotic water influx increases the oocyte volume by 25 % (*10, 13*). Since membrane stretching may account for no more than 5 % area increase (*14*), "additional" membrane material is required to explain the corresponding 16 % increase in oocyte surface area (spherical shape assumed). It comes from microvilli and foldings of the oolema that have a nine fold larger surface area than a sphere with the size of the oocyte (*10*). The partial unfolding of those microvilli and foldings increases P_{UL} because the complete volume that they enclose belongs to the unstirred layers. That is, in swollen oocytes (i) average w_{UL} is decreased and diffusion out of the foldings or into the microvilli is accelerated because these structures are smaller and (ii) a larger part of the oocyte surface gets directly exposed to the osmotic gradient. The final oocyte volume increases with on n, i.e. with P_f (*10, 13*). Thus, the smallest w_{UL} (or largest P_{UL}) is found the oocytes with the largest increase in volume. If P_{UL} increases during swelling, P_a must also be time dependent. That is, P_a cannot asymptotically approach a fixed value and its failure to do so cannot be taken as evidence for missing unstirred layer effects.

In addition, an increasing P_{UL} must also increase the osmotic gradient (*15*) that is "seen" by the AQP1 molecules. In turn, the osmotic water flux must increase out of proportion to the osmotic gradient. That is exactly what has been observed in the experiment: AQP1-expressing oocytes swelled more rapidly than predicted by van't Hoff's law (*10, 13*).

Alignments of various aquaporin structures

We aligned the bovine AQP1 (PDB #1J4N), the AQPZ (PDB #1RC2), and the GlpF (PDB #1FX8) structures to the yeast AQP structure (PDB #3Z0J) (Fig. S8). We did not use the structure of the human AQP1 (PDB #1H6I) because of its smaller resolution.

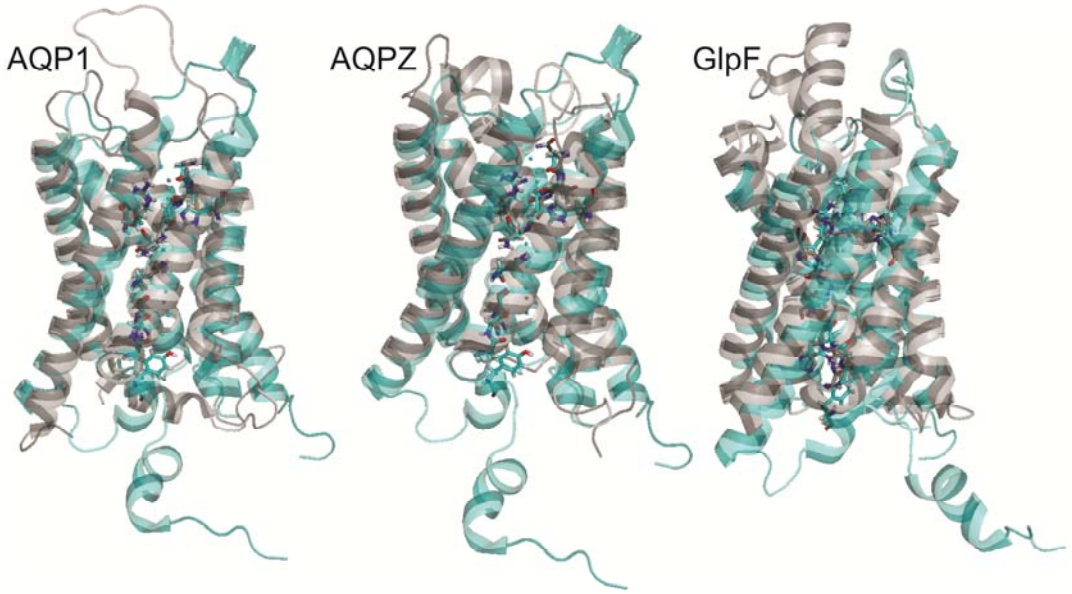

Fig. S8. The yeast AQP1 structure is in cyan, the aligned structures are in grey. H-bond forming residues from the yeast AQP1 structure are shown as cyan sticks. Aligned residues from AQP1, AQPZ and GlpF are represented as grey sticks. Single file waters present in the respective structures are shown as cyan and grey dots.

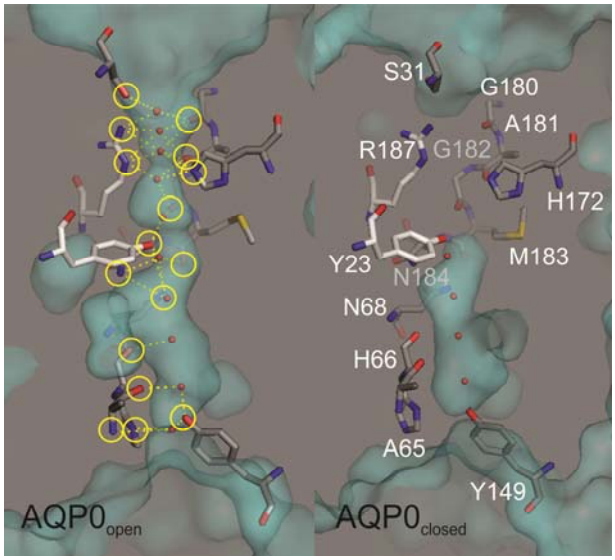

Fig. S9. Water-filled cavities in the open and closed structures of AQP0. The yellow circles highlight pore lining residues that may form hydrogen bonds (dotted lines) with single file water molecules. The yeast AQP1 structure served as a template to find the positions of single file water molecules (red dots)..

Reference List

1. K. Matsuzaki *et al.*, *Biochimica et Biophysica Acta (BBA) - Biomembranes* **1467**, 219 (2000).
2. W. M. M. Yunus, *Appl. Opt.* **31**, 2963 (1992).
3. N. Berger, A. Sachse, J. Bender, R. Schubert, M. Brandl, *Int. J. Pharm.* **223**, 55 (2001).
4. F. Zhu, E. Tajkhorshid, K. Schulten, *Biophys. J.* **83**, 154 (2002).
5. F. Q. Zhu, E. Tajkhorshid, K. Schulten, *Phys. Rev Lett.* **93**, (2004).
6. M. Hashido, A. Kidera, M. Ikeguchi, *Biophys. J.* **93**, 373 (2007).
7. B. L. de Groot, H. Grubmuller, *Science* **294**, 2353 (2001).

8. E. Tajkhorshid *et al.*, *Science* **296**, 525 (2002).
9. T. Walz, B. L. Smith, M. L. Zeidel, A. Engel, P. Agre, *J. Biol. Chem.* **269**, 1583 (1994).
10. G. A. Zampighi *et al.*, *J Membr. Biol.* **148**, 65 (1995).
11. L. Erokhova, A. Horner, P. Kugler, P. Pohl, *J. Biol. Chem.* **286**, 39926 (2011).
12. Z. Petrasek, P. Schwille, *Biophys. J.* **94**, 1437 (2008).
13. G. Chandy, G. A. Zampighi, M. Kreman, J. E. Hall, *J. Membr. Biol.* **159**, 29 (1997).
14. E. Evans, W. Rawicz, *Phys. Rev Lett.* **79**, 2379 (1997).
15. P. Pohl, S. M. Saparov, Y. N. Antonenko, *Biophys. J.* **75**, 1403 (1998).